A comparative study of riverine ^{137}Cs dynamics during high-flow events at three contaminated river catchments in Fukushima.

Takuya Niida[1], Yoshifumi Wakiyama[2]*, Hyoe Takata[2], Keisuke Taniguchi[3], Honoka Kurosawa[4], Kazuki Fujita[5], Alexei Konoplev[2]

1. KANSO TECHNOS CO., LTD.
2. Institute of Environmental Radioactivity, Fukushima University, Japan
3. National Institute of Technology, Tsuyama College, Japan
4. Graduate school of Symbiotic System Science and Technology, Fukushima University, Japan
5. Fukushima Prefectural Centre for Environmental Creation, Japan

*Corresponding author: Yoshifumi Wakiyama
Affiliation: Institute of Environmental Radioactivity, Fukushima University,
Address: 1 Kanayagawa, Fukushima city, 960-1296, Japan
Tel +081 (24) 503-2978
E-mail: wakiyama@ipc.fukushima-u.ac.jp

Graphical Abstract

Riverine ^{137}Cs dynamics during high-flow events

Three events on three river catchments

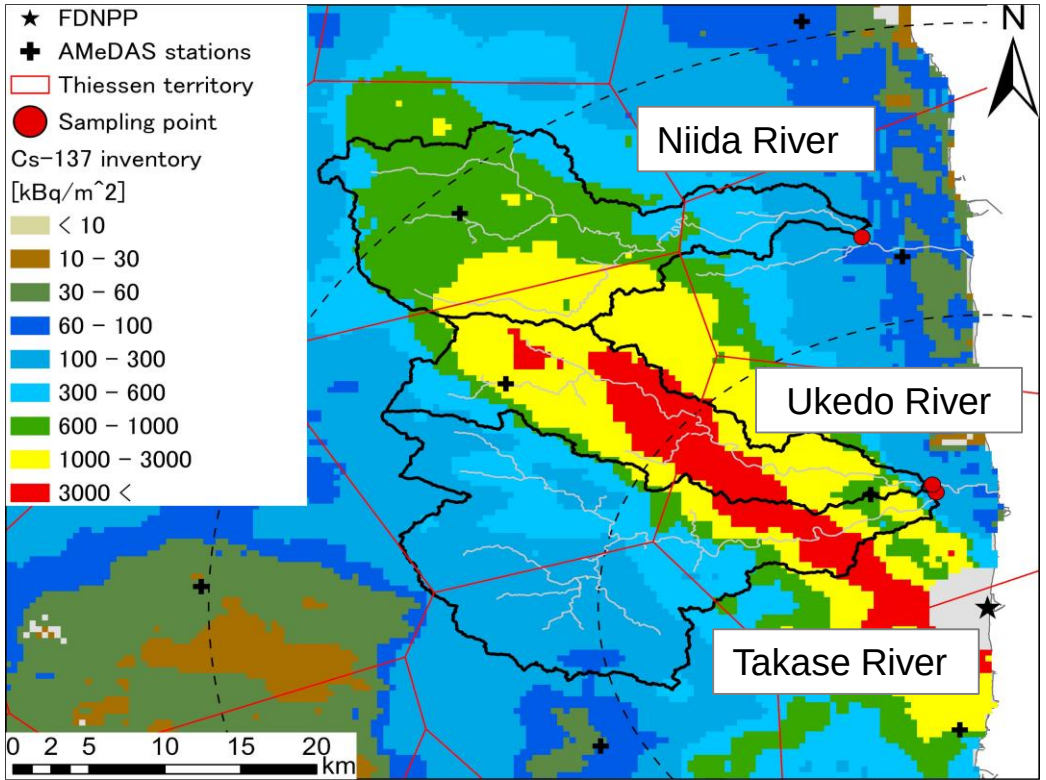

Variation in ^{137}Cs concentrations

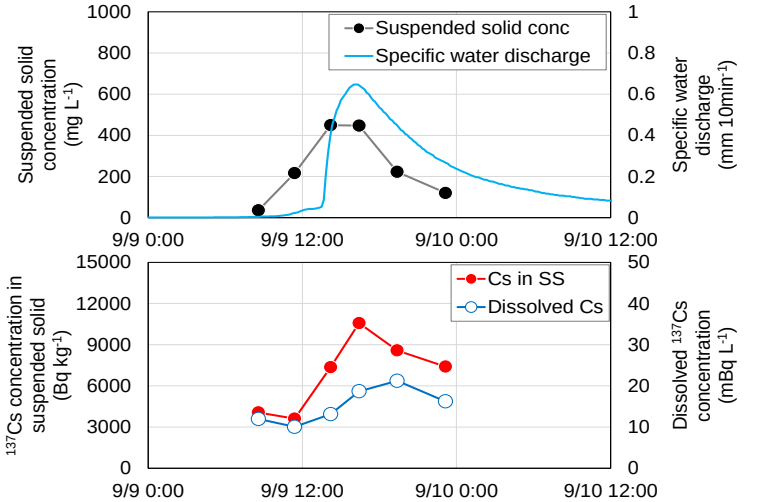

^{137}Cs flux to ocean

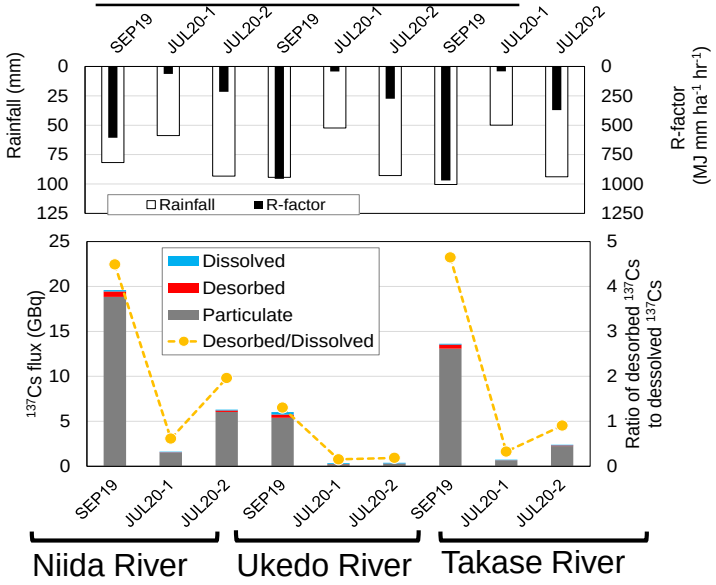

Highlights

Riverine ^{137}Cs was measured in three rivers during three high-flow events

Riverine ^{137}Cs concentrations reflect the spatial pattern of ^{137}Cs in catchments

Catchments with greater forest cover export less particulate ^{137}Cs

^{137}Cs desorbed from suspended solids exceeds dissolved ^{137}Cs flux in erosive events

Abstract

This study presents the temporal variations in riverine ^{137}Cs concentrations and fluxes to the ocean during high-flow events in three coastal river catchments contaminated by the Fukushima Daiichi Nuclear Power Plant accident. River water samples were collected at points downstream in the Niida, Ukedo, and Takase Rivers during three high-flow events that occurred in 2019–2020. Variations in both the dissolved ^{137}Cs concentration and ^{137}Cs concentration in suspended solids appeared to reflect the spatial pattern of the ^{137}Cs inventory in the catchments, rather than variations in physico-chemical properties. Negative relationships between the ^{137}Cs concentration and δ^{15}N in suspended sediment were found in all rivers during the intense rainfall events, suggesting an increased contribution of sediment from forested areas to the elevated ^{137}Cs concentration. The ^{137}Cs flux ranged from 0.33 to 18 GBq, depending on the rainfall erosivity. The particulate ^{137}Cs fluxes from the Ukedo River were relatively low compared with the other two rivers and were attributed to the effect of the Ogaki Dam reservoir upstream. The ratio of ^{137}Cs desorbed in seawater to ^{137}Cs in suspended solids ranged from 2.8% to 6.6% and tended to be higher with a higher fraction of exchangeable ^{137}Cs. The estimated potential release of ^{137}Cs from suspended solids to the ocean was 0.048–0.57 GBq, or 0.8–6.2 times higher than the direct flux of dissolved ^{137}Cs from the river. Episodic sampling during high-flow events demonstrated that the particulate ^{137}Cs flux depends on catchment characteristics and controls ^{137}Cs transfer to the ocean.

Keywords: ^{137}Cs, δ^{15}N, desorption, land use, suspended solid

1. Introduction

The large amount of rainfall and steep topography in Fukushima, compared with other areas contaminated by nuclear disasters, results in frequent high-flow events that redistribute ^{137}Cs in the terrestrial environment (e.g., Evrard et al., 2015; Konoplev et al., 2016; 2018). During high-flow events triggered by huge rainstorms, most of this ^{137}Cs is exported in particulate form (Yamashiki et al., 2014; Hayashi et al., 2016; Nakanishi et al., 2021). Yamashiki et al. (2014) show that 61% of the annual ^{137}Cs wash-off in the Abukuma River basin between August 2011 and May 2012 occurred during a single rainstorm. Hayashi et al. (2016) estimated the ^{137}Cs wash-off in the Uda River basin during a rainstorm in 2015 as 0.30% of the total ^{137}Cs inventory in the entire basin, which exceeded the annual ^{137}Cs wash-off in 2014. Efforts have been made to reproduce the ^{137}Cs wash-off during high-flow events at various spatiotemporal scales using numerical simulations (e.g., Kinouchi et al., 2015; Sakuma et al., 2017, 2019). Much effort has been made to quantify the ^{137}Cs redistribution in terrestrial areas.

Riverine ^{137}Cs dynamics during high-flow events are important for riverine ^{137}Cs dispersion to ocean environments. Studies have attempted to reproduce the long-term riverine ^{137}Cs discharge to the ocean (Tsumune et al. 2020) and event-based dispersion of particulate ^{137}Cs in coastal areas (Kamidaira et al. 2021). These simulations evaluated the dissolved and particulate ^{137}Cs discharges separately. However, recent studies of ^{137}Cs in coastal seawater indicated that particulate ^{137}Cs exported via rivers during a huge rainstorm increased the dissolved ^{137}Cs concentration in seawater, which was attributed to ^{137}Cs desorption resulting from ion exchange between suspended solids (SS) and

seawater (Takata et al., 2020, 2021). Takata et al. (2020) reported that the dissolved ^{137}Cs concentration in nearshore seawater increased immediately after Typhoon Hagibis in 2019, and ^{137}Cs desorbed from SS accounted for approximately 30% of the dissolved ^{137}Cs. Understanding riverine ^{137}Cs dynamics may improve the predictability of ^{137}Cs dispersion in oceanic environments.

Studies of the temporal variation in the dissolved ^{137}Cs concentration in rivers under high-flow conditions have important implications for ^{137}Cs dynamics (e.g., Ueda et al., 2013; Shinomiya et al., 2014; Hashimoto et al., 2015; Murakami et al., 2016; Tsuji et al., 2016; Iwagami et al., 2017). A high dissolved ^{137}Cs concentration during rainstorms was observed in forested catchments and was attributed to ^{137}Cs leaching from organic matter in the forest litter layer (e.g., Tsuji et al., 2016; Iwagami et al., 2017). However, those studies evaluated relatively small river catchments located in forested headwater catchments. Wakiyama et al. (in press) assessed the minimum dissolved ^{137}Cs concentration at peak water discharge during two high-flow events midstream of the Abukuma River. Because of the dependencies of hydrological processes and sediment dynamics in river basins in Japan (e.g., Asano et al. 2018a, 2018b), it would be worth testing the applicability of the findings for small river catchments to large river catchments quantitatively.

Compared with dissolved ^{137}Cs, factors controlling particulate ^{137}Cs have not been fully discussed. It is often stated that the particle size distribution controls the ^{137}Cs concentration in SS (He and Walling, 1996, Yoshimura et al. 2015a). However, several observations during high-flow events did not necessarily reveal proportionality between

the particle size distribution and ^{137}Cs concentration in SS (Hashimoto et al., 2015; Wakiyama et al., in press). Although the organic matter content is another potential cause of the variation in ^{137}Cs concentration (Naulier et al., 2017), there is no field evidence for the effect of organic matter in high-flow events. As majority of ^{137}Cs transported in particulate form, variations in ^{137}Cs concentration in SS and its controlling factors should be high on agenda.

The land use of catchments might be important for determining riverine ^{137}Cs dynamics. Plot-scale observations found differences in ^{137}Cs wash-off with different land use (e.g., Yoshimura et al., 2015b; Wakiyama et al., 2019). Wakiyama et al. (2019) found that the ^{137}Cs concentration in eroded sediment was three times higher from a forested area than from farmland. Based on observations of 29 river catchments in the Fukushima area, Taniguchi et al. (2019) observed an increased particulate ^{137}Cs flux from river catchments with predominant farmland, paddy fields, and urban areas. The change in the contribution of each land use component during high-flow events should cause variation in the ^{137}Cs concentration in SS. Several authors used carbon and nitrogen stable isotopes to estimate the contributions of sediment sources to riverbed (Laceby et al., 2016a) and reservoir bottom (Huon et al., 2018) sediment. The use of these stable isotopes may help the interpretation of riverine ^{137}Cs dynamics. Regarding the impact on oceanic environments, the contributions from different land uses may also influence the magnitude of ^{137}Cs desorption, which depends on the properties of SS (Takata et al., 2015).

From the above discussion, episodic sampling campaigns at downstream points in river catchments and comparative analyses may enable the discussion of riverine ^{137}Cs

dynamics and their influence on ocean environments. This study presents the results of a sampling campaign at downstream points in three radiologically contaminated catchments during three different high-flow events. Based on the temporal variation in the particulate and dissolved ^{137}Cs concentrations in the river water and the magnitude of the ^{137}Cs fluxes from the catchments, we discuss the factors controlling riverine ^{137}Cs concentrations by testing their correlations with the physico-chemical properties of water and SS and by investigating their relationship with stable nitrogen and carbon isotopes. Furthermore, we evaluated the ^{137}Cs flux, including the desorption of ^{137}Cs from suspended sediment in the ocean, by coupling hydrological datasets and laboratory experiments.

2. Materials and Method

2.1. Study site

The study sites were the Niida, Ukedo, and Takase River basins in the Hamadori area, Fukushima Prefecture; the sampling points in the three rivers were in Haramachi, Kiyobashi, and Takase districts, respectively (Figure 1). These river basins were highly contaminated by the Fukushima Daiichi Nuclear Power plant accident. Table S1 shows the characteristics of each river catchment. The areas of the Niida, Ukedo, and Takase River catchments were 206, 143, and 262 km^2, respectively. The respective mean ^{137}Cs inventories based on the fourth airborne survey in the Niida, Ukedo, and Takase River catchments were 853, 2359, and 701 kBq m^{-2}. The forest covers in the respective catchments were 67.9%, 79.7%, and 83.3%. The upper Niida River catchment was subject

to decontamination during mainly in 2014–2016. The Ogaki Dam reservoir, midstream of the Ukedo River, has a catchment area of 110 km^2 and mean ^{137}Cs inventory of 2360 kBq m^{-2} (Funaki et al., 2020). The spatial land use patterns in the three river catchments are similar. The downstream portions are in coastal areas and dominated by residences and agricultural land. The upstream portions in the Abukuma Highlands have dispersed agricultural land. The midstream portions between the highlands and coastal plain are dominated by forested areas on steep slopes (Figure S1).

2.2. River water sampling

River water was sampled at the three sites during three high-flow events on 9–10 September 2019 (SEP19), 14–21 July 2020 (JUL20-1), and 28–29 July 2020 (JUL20-2). SEP19 was triggered by Typhoon Faxai, JUL20-1 by prolonged rainfall during the East Asian rainy season, and JUL20-2 by intensive rainfall at the end of the East Asian rainy season. The R-factor in the Revised Universal Soil Loss Equation was calculated using the Rainfall Intensity Summarization Tool (United States Department of Agriculture, 2013) following Laceby et al. (2016b). Table 1 shows the catchment mean rainfall and R-factor based on the Thiessen territory created by the locations of Japan Meteorological Agency weather stations. Although the mean catchment rainfall amount was similar in SEP19 and JUL20-2, the SEP19 event R-factor was about three times higher than that of JUL20-2. Water height (m) at 10-minute intervals was downloaded from the Fukushima Prefecture website (http://kaseninf.pref.fukushima.jp/gis/) and converted into water

discharge, Q (m^3 s^{-1}), based on a water height and water discharge curve (H–Q curve). The Q was converted to specific water discharge, SWD (mm 10 min^{-1}).

In these events, 30–40 L river water was collected using a 10-L polyethylene bucket from bridges close to the hydrological observation points. Six to eight river water samples were collected per event per site (Figure 2). The sample ID and sampling time were found in Tables S2 and S3.

2.3. Sample processing and analyses

The sampled water was placed in a 50 L barrel and left for 1–2 days to allow most of the SS to settle to the bottom of the barrel. Then, the supernatant was filtered using a 0.45-μm-mesh membrane filter, and the captured solids were transferred to an evaporation dish. The SS on the filter and barrel bottom was combined in the evaporation dish. The integrated SS sample was dried at 50°C and then homogenized and disaggregated carefully in a mortar so as not to destroy the sediment particles. The SS concentration, SSC (mg L^{-1}), was calculated by dividing the SS weight by the volume of sampled water. Filtered water was passed through an ANFEZH column, an absorbent consisting of Prussian blue absorbent, to immobilize the dissolved ^{137}Cs, as described previously (Konoplev et al., 2021).

The integrated SS were measured to obtain the ^{137}Cs concentration in SS, Cs_{ss} (Bq kg^{-1}). The ^{137}Cs concentration in the ANFEZH was measured to obtain the dissolved ^{137}Cs concentration, Cs_{dis} (mBq L^{-1}). All ^{137}Cs concentration measurements were performed using standard electrode coaxial Ge detectors (GC4020, Canberra, USA) with

a relative efficiency of 42.6% at the Institute of Environmental Radioactivity, Fukushima University. Measurements had a minimum statistical error of < 5% for ^{137}Cs in SS and < 10% for dissolved ^{137}Cs. An apparent distribution coefficient, K_d (L kg^{-1}) was calculated by dividing the Cs_{ss} by the Cs_{dis}.

The particulate and dissolved ^{137}Cs fluxes (Bq) were estimated based on the ^{137}Cs concentrations and hydrological data. Each event was separated into 6 or 8 time spans, depending on the number of samples in the event. The particulate ^{137}Cs flux was obtained by multiplying SS discharge, a product of total water discharge and SSC, in each time span by the corresponding Cs_{ss}. Similarly, the dissolved ^{137}Cs flux was obtained by multiplying the water discharge in each time span by the corresponding Cs_{dis}. Due to difference in sampling interval among the events, we compared the ^{137}Cs fluxes in 48 hours before and after time of water peak discharge, i.e., 24 hours before the peak and 24 hours after the peak.

The SS samples were further analyzed to determine the carbon contents and particle size distribution. The total carbon content in SS was measured using the TOC-L CSH (Shimadzu, Japan). The particle size distribution was also measured using the Mastersizer 3000 (Malvern Panalytical, UK). The particles ranging from 0.05 to 3 mm were scanned and classified into 51 categories. The volumetric ratio of the scanned range was converted into a specific surface area, SSA (m^2 g^{-1}) by assuming spherical sediment particles. Portions of the filtrates were used to measure the concentrations of major cations (K^+, Na^+, Ca^{2+}, and Mg^{2+}) by ion chromatography (DIONEX 1100, Thermo Fisher Scientific, USA).

To evaluate the contributions of sediment sources, the stable isotope of carbon and nitrogen, i.e., $\delta^{13}C$ and $\delta^{15}N$ (‰), in SS were measured. The SS samples were packed in tin foil and then placed in a desiccator with concentrated HCl to remove the carbonates. FLASH2000–ConFlo IV–DELTA V ADVANTAGE (Thermo Fisher Scientific) was used for the analyses. Reference standards of L-alanine, L-proline, and L-tyrosine provided by the Japan Chemical Analysis Center were measured to calibrate the $\delta^{13}C$ and $\delta^{15}N$ in SS samples.

2.4. Desorption and speciation of ^{137}Cs

Five SS samples collected peak water discharge (ND-SEP19-3, ND-JUL20-2-3, UD-SEP19-3, TS-SEP19-3, and TS JUL20-2-4), were selected because the amounts of these SS were sufficient for both the desorption experiments and subsequent sequential extraction. Seawater filtered through a 0.45-μm membrane filter was used for the extraction experiments; the dissolved ^{137}Cs concentration in the seawater was 2.7 mBq/L. The desorption experiment was performed following the methods of Takata et al. (2015, 2021). Briefly, the SS samples were placed in 18 L containers with seawater to achieve a solid-to-liquid ratio of 1 g to 5 L in an 18-L container and shaken for 30 minutes or 1 day. Then, the SS samples were separated by filtration through a 0.45-μm pore size membrane filter. The ^{137}Cs in the seawater after shaking was co-precipitated with ammonium molybdophosphate (AMP) to quantify the dissolved ^{137}Cs concentration. The desorption ratio was calculated by dividing the dissolved ^{137}Cs concentration in the seawater by the ^{137}Cs concentration in SS.

To evaluate the mobility of SS-borne ^{137}Cs, its speciation, i.e., the composition of ^{137}Cs in the exchangeable, organic-bound, and particle-bound fractions, was evaluated in sequential SS extraction experiments performed following the procedure of Tsukada and Ohse (2016). Briefly, 1 mol L^{-1} CH_3COONH_4 was used to extract the exchangeable fraction, and 30% H_2O_2 with HNO_3 was used to extract the organic fraction. Each leached solution was transferred to a plastic container, and the ^{137}Cs concentration was measured using Ge gamma-ray spectrometry. The remaining fraction was assumed to be strongly bound to sediment particles, i.e., the particle-bound fraction.

3. Results and Discussion

3.1. Temporal variation in the riverine ^{137}Cs concentrations

Figure 3 shows the temporal variations in the Cs_{ss}, the Cs_{dis}, and SSC. Table 3 lists all data of the Cs_{ss}, the Cs_{dis}, and SSC. In the Niida River, the ^{137}Cs concentration in SS peaked during the peak discharge phase in SEP19, whereas increasing trends were found throughout JUL20-1 and JUL20-2. There was no common trend for the Cs_{dis}, which tended to be synchronized with the specific water discharge in SEP19 but was relatively stable during JUL20-1 and JUL20-2. The stable concentrations during these two events in 2020 might reflect the impact of Typhoon Hagibis in 2019. The Ukedo River had low SSCs throughout the three events, compared with the other two rivers. This low SSC might be influenced by the Ogaki Dam upstream. Its ^{137}Cs concentration in SS peaked after a few hours of peak flow in SEP19, while the ^{137}Cs in SS did not show much variation in JUL20-1 and JUL20-2. The Cs_{dis} tended to increase with the specific water

discharge in SEP19. The Takase River had the highest ^{137}Cs concentration in SS before the peak water discharge in SEP19 and JUL20-2. The ^{137}Cs concentration in SS obviously decreased during the peak discharge phase. The Cs_{dis} tended to decrease with time during all three events. However, the temporal patterns in the riverine ^{137}Cs concentrations differed according to the event, even within the same river catchment.

To evaluate the response of the ^{137}Cs concentrations to sediment and water discharge, we plotted the normalized Cs_{dis} and normalized Cs_{ss} against the logarithms of the specific discharge and SSC, following the analyses by Tsuji et al. (2016) (Figure 4). The Niida River showed significant positive correlations or all four relationships ($p < 0.05$). The Ukedo River had a significant positive correlation between SSC and the ^{137}Cs concentration in SS. The Takase River had negative correlations of the Cs_{dis} with both the SWD and SSC but positive correlations of the K_d with both the SWD and SSC.

These results differed from those of Tsuji et al. (2016), who found a positive correlation for the Cs_{dis}, but no correlation for the ^{137}Cs concentration. The negative correlation for the Takase River could be explained by the spatial pattern of the ^{137}Cs inventory in the catchment. As shown in Figure 1, the Takase River catchment has a highly contaminated area downstream, whereas the other two river catchments have the most contaminated areas upstream. This situation might result in the dilution of dissolved ^{137}Cs by water upstream, with a relatively low ^{137}Cs inventory in the Takase River and the opposite for the Niida and Ukedo Rivers. The variation in the ^{137}Cs concentration might be reflected in the spatial pattern of the ^{137}Cs inventory in these river catchments. In this context, the positive correlation between the ^{137}Cs concentrations in SS and Cs_{dis}

in the Niida River could also be explained by increased contributions from upstream, with a high ^{137}Cs inventory. The difference in the range of the ^{137}Cs inventory in the catchments might explain the discrepancy with the results of Tsuji et al. (2016). The range in the ^{137}Cs inventory in our study catchments was two orders of magnitude, as shown in Figure 1, whereas that in the catchments in Tsuji et al. (2016) was within 1000–3000 Bq m^{-2}. These results suggest that the variation and spatial pattern of the ^{137}Cs inventory were reflected in the riverine ^{137}Cs concentrations in the catchments evaluated.

Interestingly, all three rivers showed positive relationships between SSC and K_d. Previous studies often found negative correlations between these parameters (e.g., Ueda et al., 2013; Murakami et al., 2016). IAEA (2020) also observed negative relationships upstream in the Mano, Niida, and Ohta Rivers, which have maximum catchment areas of 21 km^2. By contrast, Wakiyama et al. (in press) found a significant positive correlation during high-flow events midstream of the Abukuma River. These results suggest a dependency of the variation in K_d on the catchment scale.

3.2. Factors controlling the ^{137}Cs concentration

Previous studies found significant correlations of the ^{137}Cs concentrations and the apparent distribution coefficient with the physico-chemical properties of water and SS, such as the positive correlation between K^+ concentration and dissolved ^{137}Cs concentration (Tsuji et al., 2019), positive correlation between SSA and ^{137}Cs concentration in SS (Yoshimura et al., 2015a), total organic carbon-^{137}Cs concentration in SS (Naulier et al., 2017), and negative correlation between EC and K_d (IAEA, 2020),

dependencies of K_d on particle size distribution (Abrill and Fraga, 1996). Although the results of Figure 3 suggest that the spatial pattern of the ^{137}Cs inventory is reflected in the variation in the ^{137}Cs concentration, the physico-chemical properties of water/sediment might have determined the ^{137}Cs concentrations; it is worth examining these relationships. Table 2 lists the correlation coefficients between the ^{137}Cs concentrations or apparent K_d with representative physico-chemical parameters. We could not find any attributes that explained the variation in the ^{137}Cs concentrations and distribution coefficients in all rivers. Among the relationships, the correlation coefficients between the EC and Cs_{dis} were positive for all three events in the Niida River but were negative for all events in the Takase River. Although SSA was believed to control the ^{137}Cs concentration in SS (e.g., He and Walling, 1996), our results disagreed with those findings. Similar to the Cs_{dis}, the ^{137}Cs concentration in SS could not be explained by a single physico-chemical property, even one that was significant for low-flow conditions. It is reasonable to postulate that the temporal variation in these physico-chemical properties also varied with the catchment characteristics, and the complicated hydrological processes apparently hindered the synchronicity of the ^{137}Cs concentrations with any single property. These results suggest importance of consideration of the site-specific hydrological processes and sediment dynamics of river catchments.

To discuss the role of catchment land use, we investigated the relationship between the ^{137}Cs concentration in SS and $\delta^{15}N$, as an index of the contribution of sediment sources based on data in Laceby et al. (2016a) (Figure 5). Table S3 shows all data of the $\delta^{13}C$ and $\delta^{15}N$. Although both $\delta^{13}C$ and $\delta^{15}N$ were measured, we decided to

use $\delta^{15}N$ here because there was a negative shift in the $\delta^{13}C$ of the sediment source sample, as described by Laceby et al. (2016a) (Figure S1). The ^{137}Cs concentration tended to be increase with decreasing $\delta^{15}N$ concentration, although this correlation was not statistically significant. This relationship suggests that the high contribution of forested area increases the ^{137}Cs concentration in SS based on a comparison of the mean values of $\delta^{15}N$ in the source area. This concurs with plot-scale ^{137}Cs wash-off observations (e.g., Yoshimura et al., 2015b; Wakiyama et al., 2019), showing 1.4–3 times higher ^{137}Cs concentrations in eroded sediment in forested areas compared with farmland. We speculate that the increased SS load from forested areas increased the ^{137}Cs concentration in SS.

The increased contribution from forested areas could be explained by a variable source area concept; i.e., intensive rainfall results in an expanded contribution area of runoff water (e.g., Hewlett and Hibbert, 1967). Previous studies of global fallout ^{137}Cs showed that soils in upslope areas were barely eroded and were expected to maintain high ^{137}Cs concentrations (e.g., Fukuyama et al., 2001; Wakiyama et al., 2010). However, the expanded runoff area during a rainfall event washed surface soil downstream, resulting in an increased ^{137}Cs concentration in SS. Future numerical studies of these hydrological processes will improve our understanding of ^{137}Cs dynamics.

By contrast, no such relationships were clear for the Niida and Takase Rivers for JUL20-1 and JUL20-2. For JUL20-1, a wide range of $\delta^{15}N$ and stable ^{137}Cs concentrations were observed in the Niida and Takase Rivers. As the rainfall erosivity was low compared with the other two events, little severe soil erosion was expected. Plausibly, the riverbed or riverbank was the main sediment source during the events. The relationships in the

Niida and Takase Rivers in JUL20-2 were not straightforward. Both rivers had a low $\delta^{15}N$, close to 0‰, with a low ^{137}Cs concentration, unlike those during SEP19. These two values infer that forest in the midstream area with a low ^{137}Cs inventory, as shown in Figure 1, was the dominant sediment source during sampling. This is indeed the case for the Takase River; sharp decreases in Cs_{ss} of two samples after peak discharge were found in JUL20-2 as shown in Figure 3.

In contrast to the other two rivers, high stable values of $\delta^{15}N$ were found in the Ukedo River in both JUL20-1 and JUL20-2, with little variation in Cs_{ss}. We postulate that the Ogaki Dam trapped SS from the highly contaminated upstream area, and that the main sediment source was cultivated, decontaminated land downstream, in these events. Our stable isotope signature analyses demonstrated that the spatial distribution of ^{137}Cs and land use composition in the catchment control the variation in the ^{137}Cs concentration in SS during high-flow events.

3.3. ^{137}Cs flux from rivers and desorption in the ocean

Based on the ^{137}Cs concentrations and ^{137}Cs desorption experiment, we estimated the ^{137}Cs flux, including ^{137}Cs desorption, from the river catchments (Table 3). The total ^{137}Cs flux ranged from 0.325 to 19.0 GBq, or 0.00014 to 0.010% of the total ^{137}Cs deposited in the catchments. The particulate ^{137}Cs flux ranged from 0.32 to 18.8 GBq, and the dissolved ^{137}Cs flux ranged from 0.061 to 0.273 GBq. The total ^{137}Cs flux accounted for 0.001–0.034% of the total ^{137}Cs in the catchments. The Niida River exported the most ^{137}Cs, followed by the Takase River and then Ukedo River. The

percentage of the total ^{137}Cs flux to the total ^{137}Cs deposited in the Ukedo River catchment was one order of magnitude lower than those in the other two rivers. The Ogaki Dam reservoir appeared to mitigate the ^{137}Cs flux by trapping discharged sediments. Nakanishi et al. (2021) found a 14 times higher sediment discharge from the Takase River than from the Ukedo River during Typhoons Hagibis and Bualoi in 2019. Hayashi and Tsuji (2020) reported ^{137}Cs storage rates in the dam reservoir of 84–95% based on the difference in observed ^{137}Cs inflow and outflow for the Matsugabo Dam reservoir in the Uda River catchment. The particulate ^{137}Cs flux of one magnitude lower in the Ukedo River concurs with their results. In comparison, the magnitude of the dissolved ^{137}Cs flux was similar to those in the other two rivers. Funaki et al. (2020) estimated the dissolved ^{137}Cs flux from the Ogaki Dam reservoir to be 1.0–2.2 $\times 10^{10}$ Bq per year. In terms of the ratio of the rainfall amount during these events to the annual rainfall, values of 0.18 and 0.22 GBq are reasonable. The Ogaki Dam reservoir likely contained trapped SS at the bottom and mitigated sediment discharge and particulate ^{137}Cs during high-flow events.

The particulate ^{137}Cs flux clearly increased with the event R-factor, rather than with the rainfall amount, for all three catchments (Figure 6). Although statistical significance could not be evaluated because of insufficient observations, the both the particulate and dissolved ^{137}Cs fluxes were more proportional to the R-factor than to the catchment mean precipitation. When examining the sensitivity of the particulate ^{137}Cs flux to the R-factor using the slope of the regression, the Niida River showed a relatively sharp increase in the particulate ^{137}Cs flux, followed by the Takase River and then Ukedo River. The greater sensitivity of the Niida River could be attributed to the smaller ratio of

forest cover in the catchment. Based on soil erosion observations, Wakiyama et al. (2019) reported a 3–50 times higher ^{137}Cs discharge from farmland than forest. Taniguchi et al. (2019) indicated that a high ratio of forested area in a catchment resulted in a smaller ^{137}Cs flux. As more than 95% of the ^{137}Cs was transported in a particulate form, using the R-factor of other erosivity parameters yields more accurate estimates compared with using the rainfall amount. The low sensitivity of the Ukedo River is due to the effect of the Ogaki Dam, as discussed above.

The above datasets of the particulate ^{137}Cs flux enabled us to estimate the potential magnitude of the desorption of ^{137}Cs from SS, as demonstrated by Takata et al. (2021). Table 4 shows the results for sea water extraction for ^{137}Cs desorption and the sequential extraction for ^{137}Cs speciation. The desorption percentage was slightly higher in the 30-minute experiment than in the 1-day experiment, ranging from 2.8% to 6.6%. The magnitude of ^{137}Cs desorption also agreed with that reported by Takata et al. (2020, 2021). The values for the speciation of ^{137}Cs were higher than those reported by Tsukada and Ohse (2016): 0.9–1.5% for the exchangeable faction and 1.8–4.1% for the organically bound ^{137}Cs fraction in SS under low-flow conditions. The difference might be because the SS samples were derived mainly from forest area, as discussed for Figure 5. The desorption ratio appeared to be high when the proportion of the ion-exchange fraction was high, although the correlation was not significant. The slope of the approximate linear equation between the results of the 1-day desorption experiment and the ion-exchange fraction was close to 1, suggesting that the ion-exchange fraction was desorbed in the 1-day desorption experiment. These results confirmed that ^{137}Cs in the exchangeable

fractions is desorbed in the ocean and revealed the magnitude of ^{137}Cs desorption from SS.

By multiplying the percentage of ^{137}Cs desorption by the particulate ^{137}Cs flux, the estimated potential range of ^{137}Cs desorbed from SS in the ocean was 0.022–0.57 GBq (Table 5). The ratio of desorbed ^{137}Cs to dissolved ^{137}Cs ranged from 0.12 to 6.2, and the ratios during SEP19 were the highest for all three rivers. The large particulate ^{137}Cs flux during this intensive rainfall event resulted in a relative increase in the amount of desorbed ^{137}Cs. In the case of the Abukuma River after Typhoon Hagibis, the ratio of desorbed ^{137}Cs to dissolved ^{137}Cs reached 130 due to the considerable particulate ^{137}Cs flux (Takata et al., 2021). Intensive rainfall results in large amount of desorption of ^{137}Cs from SS, which may increase the dissolved ^{137}Cs concentration in near-shore seawater. These results underline the importance of particulate ^{137}Cs dynamics for both terrestrial and oceanic environments.

4. Conclusion

We examined the riverine ^{137}Cs dynamics during high-flow events and their influence on ocean environments. The temporal variation in the ^{137}Cs concentration differed according to the event, even in the same river catchment, and appeared to reflect the spatial distribution of the ^{137}Cs inventory in the catchments, rather than the influence of the dynamics of the physico-chemical properties of water and SS. The relationship between δ^{15}N and the ^{137}Cs concentration in SS suggested that SS discharged from forested areas during intensive rainfall events increased the ^{137}Cs concentration in SS.

From the results, we postulate that the spatial distribution of the ^{137}Cs inventory and land use composition in catchments control the variation in riverine ^{137}Cs concentrations during high-flow events in relatively large river catchments with different land uses.

The differences in the land use composition of the catchments were also reflected in the ^{137}Cs fluxes. The sensitivity of the particulate ^{137}Cs flux to the rainfall erosivity was low in a highly forested catchment. Our results demonstrated that a dam reservoir mitigated ^{137}Cs exportation via sediment trapping. The estimated percentage of desorbed ^{137}Cs relative to particulate ^{137}Cs was 2–6% based on desorption experiments. These values roughly agreed with the percentage of ^{137}Cs in the exchange fraction in SS. The amount of ^{137}Cs desorbed in the ocean depended on the particulate ^{137}Cs flux and exceeded the dissolved ^{137}Cs flux from terrestrials during intensive rainfall events. Hence, the particulate ^{137}Cs dynamics are important not only for ^{137}Cs redistribution in terrestrial areas but also for ^{137}Cs diffusion in the ocean. Further comparative studies of various high-flow events in different catchments, and numerical simulations based on such observations, will improve our understanding of riverine ^{137}Cs dynamics.

Acknowledgement

This research was funded by the Japan Society for the Promotion of Science, Grant-in-aid for Scientific Researches (B) (18H03389), and (21H03574). Dr. Kenji Nanba and Dr. Toshihiro Wada supported the measurements of stable isotope compositions of carbon and nitrogen.

Reference

Abril, J.M., Fraga, E.F. 1996. Some physical and chemical features of variability of k_d distribution coefficients for radionuclides. *J. Environ. Radioact*. **30**, 253-270.

Asano, Y., Uchida, T., Gomi, T., Mizugaki, S., Hiraoka, M., Katsuyama, M., Niwa, S., Yokoo, Y. 2018a. Effects of Spatial Scales on Runoff / Sediment Transport in Mountain Catchments (1) - A Review of Field Observations on Catchment Area and Properties. *J. Japan Soc. Hydrol. and Water Resour*. **31**, 219 – 231. (in Japanese with English abstract). DOI: 10.3178/jjshwr.31.219.

Asano, Y., Uchida, T., Katsuyama, M., Hiraoka, M., Mizugaki, S., Gomi, T., Niwa, S., Yokoo, Y. 2018b. Effects of Spatial Scales on Runoff / Sediment Transport in Mountain Catchments (2) -Results from Intensively Studied Catchments. *J. Japan Soc. Hydrol. and Water Resour*., **31**, 232-244. (in Japanese with English abstract).

Evrard, O., Leceby, J.P., Lepage, H., Onda, Y., Cerdan, O., Aylault, S. 2015. Radiocesium transfer from hillslopes to the Pacific Ocean after the Fukushima Nuclear Power Plant accident: A review. *J. Environ. Radioact.* **148**, 92-110.

Fukuyama, T., Onda, Y., Takenaka, C., Yamamot, T. 2001. Estimation of soil erosion using a radionuclide in reservoir sediment and forest soil. *J. JSECE*, 54, 4-11. (in Japanese with English abstract)

Funaki, H., Sakuma, K., Nakanishi, T., Yoshimura, K., Katengeza, W.E. 2020. Reservoir sediments as a long-term source of dissolved radiocaesium in water system; a mass balance case study of an artificial reservoir in Fukushima, Japan. *Sci. Total. Environ*. **743**, 140668.

Hashimoto, T., Yokoyama, K., Kohno, M., Ohno, A. 2015. Transport of radiocesium depending on the particle size of suspended sediment during flood discharge. *J. Jpn Soc Civil Engineers*, Ser. B1 (Hydraulic Engineering),**71**, I_1195-I_1200. (in Japanese with English abstract).

Hayashi, S., Tsuji, H., Ito, S., Nishikiori, T., Yasutaka, T. 2016. Export of radioactive cesium in an extreme flooding event by typhoon Etau. *J. Jpn Soc Civil Engineers*, Ser. G (Environmental Research), **72**, III_37-III_43. (in Japanese with English abstract).

Hayashi, S., Tsuji, H., 2020. Role and effect of a dam on migration of radioactive cesium in a river catchment after the Fukushima Daiichi Nuclear Power Plant accident. *Global Environ. Res*. **24**, 105-113.

He, Q and Walling, D.E., 1996. Interpreting particle size effects in the adsorption of ^{137}Cs and unsupported ^{210}Pb by mineral soils and sediments. *J. Environ. Radioact*. **30**, 117-137.

Hewlett, J.D. and Hibbert, A.R. 1967: Factors affecting the response of small watersheds to precipitation in humid areas. In Sopper, W.E. and Lull, H.W., editors, Forest hydrology, New York: Pergamon Press, 275–90.

Huon, S., Hayashi, S., Laceby, J.P., Tsuji, H., Onda, Y., Evrard, E. 2018. Source dynamics of radiocesium-contaminated particulate matter deposited in an agricultural water reservoir after the Fukushima nuclear accident. *Sci Total Environ*, **612**, 1079-1090.

IAEA. 2020, Environmental transfer of radionuclides in Japan following the accident at the Fukushima Daiichi Nuclear Power Plant. IAEA-TECDOC-1927

Iwagami, S., Tsujimura, M., Onda, Y., Nishino, M., Konuma, R., Abe, Y., Hada., Pun, I., Sakaguchi, A., Kato, H., Yamamoto, M., Miyata, Y., Igarashi, Y., 2017. Temporal changes in dissolved ^{137}Cs concentrations in groundwater and stream water in Fukushima after the Fukushima Dai-ichi Nuclear Power Plant accident. *J. Environ. Radioact*. **166**, 458-465.

Kamidaira, Y., Uchiyama, Y., Kawamura, H., Kobayashi, T. Otosaka, Y. 2021. A modeling study on the oceanic dispersion and sedimentation of radionuclides off the coast of Fukushima. *J. Environ. Radioact*. **238-239**, 10672.

Kinouchi, T., Yoshimura, K., Omata, T. 2015. Modeling radiocesium transport from a river catchment based on a physically-based distributed hydrological and sediment erosion model. *J. Environ. Radioact*. **139**, 407-415.

Konoplev, A., Golosov, V., Laptev, G., Nanba, K., Onda, Y., Takase, T., Wakiyama, Y., Yoshimura, K., 2016. Behavior of accidentally released radiocesium in soil-water environment: Looking at Fukushima from a Chernobyl perspective. *J. Environ. Radioact*. **151**, 568-578.

Konoplev, A., Golosov, V., Wakiyama, Y., Takase, T., Yoschenko, V., Yoshihara, T., Parebyuk, O., Cresswell, A., Ivanov, M., Carradine, M., Nanba, K., Onda, Y. 2018. Natural attenuation of Fukushima-derived radiocesium in soils due to its vertical and lateral migration. *J. Environ. Radioact*. **186**, 23-33.

Konoplev, A., Wakiyama, Y., Wada, T., Udy, C., Kanivets, V., Ivanov, M.M., Komissarov, M., Takase, T., Goto, A., Nanba, K. 2021. Radiocesium distribution and mid-term dynamics in the ponds of the Fukushima Dai-ichi nuclear power plant exclusion zone in 2015–2019, *Chemosphere*, 265, 129058.

Laceby, JP., Huon, S., Onda, Y., Vaury, V., Evrard, O. 2016a. Do forests represent a long-term source of contaminated particulate matter in the Fukushima Prefecture? *J. Environ. Manage.*, **183**, 742-753.

Laceby, JP., Chartini, C., Evrard, O., Onda, Y., Garcia-Sanchez, L., Cerdan, O. 2016b. Rainfall erosivity in catchments contaminated with fallout from the Fukushima Daiichi nuclear power plant accident. *Hydrol. Earth Syst. Sci.*, **20**, 2467–2482.

Murakami, M., Shibayama, N., Sueki, K., Mouri, G., O, H., Nomura, M., Koibuchi, Y., Oki, T. 2016. Occurrence and partition ratios of radiocesium in an urban river during dry and wet weather after the 2011 nuclear accident in Fukushima. *Water Res*. **92**, 87-93.

Nakanishi, T., Ohyama, T., Hagiwara, H., Sakuma, K. 2021. Impact of extreme typhoon events on the fluvial discharge of particulate radiocesium in Fukushima Prefecture. *In*: Lee, J.L.; Suh, K.-S.; Lee, B.; Shin, S., and Lee, J. (eds.), *Crisis and Integrated Management for Coastal and Marine Safety. Journal of Coastal Research*, Special Issue No. 114, pp. 310–314. Coconut Creek (Florida), ISSN 0749-0208.

Naulier, M., Eyrolle-Boyer, F., Eyrolle-Boyer, P., Métivier, J.M. 2017. Particulate organic matter in rivers of Fukushima: An unexpected carrier phase for radiocesiums. *Sci. Total Environ.* **579**, 1560-1571.

Sakuma, K., Kitamura, A., Malins, A., Kurikami, H., Machida, M., Mori, K., Tada, K., Kobayashi, T., Tawara, Y., Tosaka, H. 2017. Characteristics of radio-cesium transport and discharge between different basins near to the Fukushima Dai-ichi Nuclear Power Plant after heavy rainfall events, *J. Environ. Radioact*. **169-170**, 137-150.

Sakuma, K., Nakanishi, T., Yoshimura, K., Kurikami, H., Nanba, K., Zheleznyak, M. 2019. A modeling approach to estimate the ^{137}Cs discharge in rivers from immediately after the Fukushima accident until 2017. *J. Environ. Radioact.* **208-209**, 106041.

Shinomiya, Y., Tamai, K., Kobayashi, M., Ohnuki, Y., Shimizu, T., Iida, S., Nobuhiro, T., Sawano, S., Tsuboyama, Y., Hiruta, T. 2014. Radioactive cesium discharge in stream water from a small watershed in forested headwaters during a typhoon flood event. *Soil Sci. Plant Nutr*. **60**, 765-771.

Takata, H., Hasegawa, K., Oikawa, S., Kudo, N., Ikenoue, T., Isono, S. R., Kusakabe, M., 2015. Remobilization of radiocesium on riverine particles in seawater: The contribution of desorption to the export flux to the marine environment. *Marine Chemistry*. 176, 51-63.

Takata, H., Aono, T., Inoue, M., Kaeriyama, H., Suzuki, S., Tsuruta, T., Wada, T., Wakiyama, Y. 2020. Suspended particle-water interactions increase dissolved ^{137}Cs activities in the nearshore seawater during typhoon Hagibis. *Environ. Sci. Technol.*, **54**, 10678–10687.

Takata, H., Wakiyama, Y., Niida, T., Igarashi, Y., Konoplev, A., Inatomi, N. 2021. Importance of desorption process from Abukuma River's suspended particles in increasing dissolved 137Cs in coastal water during river-flood caused by typhoons. *Chemosphere*, **281**, 130751.

Taniguchi, K. Onda, Y., Smith, H.G., Blake, W.H,. Yoshimura, K., Yamashiki, Y., Kuramoto, T., Saito, K. 2019. Transport and redistribution of radiocaesium in Fukushima fallout through rivers. *Environ. Sci. Technol.*, **53**, 12339-12347.

Tsuji, H., Nishikiori, T., Yasutaka, T., Watanabe, M., Ito, S., Hayashi, S., 2016. Behavior of dissolved radiocesium in river water in a forested watershed in Fukushima Prefecture. *J. Geophys. Res. Biogeoscience*. **121**, 2588-2599.

Tsuji, H., Ishii, Y., Shin, M., Taniguchi, K., Arai, H., Kurihara, M., Yasutaka, T., Kuramoto,T., Nakanishi, T., Lee, S., Shinano, T., Onda, Y., Hayashi, S. 2019. Factors controlling dissolved ^{137}Cs concentrations in east Japanese Rivers. *Sci. Total Environ.*, **697**, 134093.

Tsukada, H., Ohse, K. 2016. Concentration of radiocaesium in rice and irrigation water, and soil management practices in Oguni, Date, Fukushima. Integrated Environmental Assesment and Management. 12, 659-661.

Tsumune, D., Tsubono, T., Misumi, K., Tateda, y., Toyoda, y., Onda, Y., Aoyama, M. 2020. Impacts of direct release and river discharge on oceanic 137Cs derived from the Fukushima Dai-ichi Nuclear Power Plant accident. *J. Environ. Radioact*., **214-215**, 106173

Ueda, S., Hasegawa, H., Kakiuchi, H., Akata, N., Ohtsuka, Y., Hisamatsu, S. 2013. Fluvial discharges of radiocesium from watersheds contaminated by the Fukushima Dai-ichi Nuclear Power Plant accident, Japan. *J. Environ. Radioact.* **118**, 96–104.

United States Department Agriculture, 2013. Rainfall Intensity Summarization Tool (RIST), United States Department of Agriculture (USDA), Agriculture Research Service, National Sedimentation Laboratory, Oxford, Mississippi, Version 3.88. https://www.ars.usda.gov/southeast-area/oxford-ms/national-sedimentation-laboratory/watershed-physical-processes-research/research/rist/rist-rainfall-intensity-summarization-tool/, accessed 26th October 2021.

Wakiyama, Y., Onda, Y., Mizugaki, S., Asai, H., Hiramatsu, S. 2010. Soil erosion rates on forested mountain hillslopes estimated using ^{137}Cs and ^{210}Pb$_{ex}$. *Geoderma*, **159**, 39-52.

Wakiyama, Y., Onda Y., Yoshimura K., Igarashi Y., Kato H., 2019. Land use types control solid wash-off rate and entrainment coefficient of Fukushima-derived ^{137}Cs and their time dependence. *J. Environ. Radioact.*, **210**, 105990.

Wakiyama, Y., Konoplev, A., Thoa, N., Niida, T., Tsukada, H., Takase, T., Nanba, K., Golosov, V., Zheleznyak M. in press. Temporal variations in particulate and dissolved 137Cs activity concentrations in the Abukuma River during two high-flow events in 2018. *In*: Nanba, K., Konoplev, A., Wada, T. (Eds.), *Behavior of radionuclides in the environment III: Fukushima, Springer Nature Singapore Pte. Ltd.*, Singapore.

Yamashiki, Y., Onda, Y., Smith, H.G., Blake, W.H., Wakahara, T., Igarashi, Y., Matsuura, Y., Yoshimura, K., 2014. Initial flux of sediment-associated radiocesium to the ocean from the largest river impacted by Fukushima Daiichi Nuclear Power Plant. *Sci. Rep.* **4**, 3714.

Yoshimura, K., Onda, Y., Sakaguchi, A., Yamamoto, M., Matsuura, Y., 2015a. An extensive study of the concentrations of particulate/dissolved radiocaesium derived from the Fukushima Dai-ichi Nuclear Power Plant accident in various river systems and their relationship with catchment inventory. *J. Environ. Radioact.* **139**, 370–378.

Yoshimura, K., Onda, Y., Kato, H. 2015b. Evaluation of radiocaesium wash-off by soil erosion from various land uses using USLE plots. *J. Environ. Radioact.* **139**, 362-369.

Captions

Table 1. Catchment mean rainfall and event R-factor.

Table 2. Correlations of the ^{137}Cs concentration in suspended solids (Cs_{ss}), dissolved ^{137}Cs concentration (Cs_{dis}), and apparent distribution coefficient (K_d) with representative physico-chemical properties.

Table 3. The suspended solid, particulate, dissolved, and total ^{137}Cs fluxes

Table 4. Results of desorption experiment and sequential extraction

Table 5. Estimated amount of ^{137}Cs desorbed from suspended solids in the ocean and the ratio of desorbed ^{137}Cs to dissolved ^{137}Cs.

Figure 1. Spatial distribution of the ^{137}Cs inventory, land use, and slope gradient in the study catchments. The spatial distribution of the ^{137}Cs inventory is based on the fourth airborne survey by MEXT (2011). The Thiessen territory was created based on the coordination of Japan Meteorological Agency weather stations.

Figure 2. Sampling times (vertical dashed lines) of river water along with the hyetographs and hydrographs of the observed events. The hyetographs show the catchment mean rainfall amounts based on the Thiessen territory in Figure 1. The hydrograph shows the 10 minutes specific water discharge (SWD).

Figure 3. Temporal variations in the suspended solid concentration (SSC), ^{137}Cs concentration in suspended solids (Cs_{ss}), and dissolved ^{137}Cs concentration (Cs_{dis}) during the events.

Figure 4. Scatterplots of the normalized ^{137}Cs concentration in suspended sediment (normalized Cs_{ss}), normalized dissolved ^{137}Cs concentration (normalized Cs_{dis}), and K_d versus the logarithms of the specific water discharge (SWD) and suspended solid concentration (SSC). The normalized Cs_{ss} and normalized Cs_{dis} were obtained by dividing Cs_{ss} and Cs_{dis} by Catchment mean ^{137}Cs inventory, respectively. The specific water discharge (SWD) every 10 minutes during sampling was multiplied by 6 to determine the hourly specific water discharge following Tsuji et al. (2016). Broken lines indicate significant correlations.

Figure 5. Relationship between the $\delta^{15}N$ and ^{137}Cs concentrations in suspended solids (Cs_{ss}). Broken lines represent the mean concentration of $\delta^{15}N$ in soil (< 2 mm), subsoil, cultivated land, and forest, according to Laceby et al. (2016a)

Figure 6. Scatterplots of the percentages of particulate and dissolved ^{137}Cs fluxes relative to the total ^{137}Cs in catchments, and the ratio of the particulate ^{137}Cs flux to the total ^{137}Cs flux versus the catchment mean rainfall and event R-factor.

Supplementary materials

Table S1. Characteristics of the river catchments

Table S2. Data of suspended solid concentration (SSC), ^{137}Cs concentration in uspended solids (Cs_{ss}), dissolved ^{137}Cs concentration (Cs_{dis}), apparent distribution coefficient (K_d).

Table S3. Data of $\delta^{13}C$ and $\delta^{15}N$.

Figure S1. Relationship between $\delta^{13}C$ and $\delta^{15}N$ in suspended solids and soils in the sediment souce area. The values for soils were derived from Lacyby et al. (2016a)

Table 1. Catchment mean rainfall and event R-factor

		Weather station							Catchment		
		Soma	Iitate	Haramachi	Tsushima	Namie	Kawauchi	Funehiki	Niida River	Ukedo River	Takase River
Ratio to entire catchment (%)	Niida River	1	68	17	14	0	0	0			
	Ukedo River	0	0	0	68	32	0	0			
	Takase River	0	0	0	41	26	1	32			
Total rainfall (mm)	SEP19	27.5	90	34	104.5	73	118	83	81.8	94.3	100.4
	JUL20-1	134	81	102.5	62	67.5	49.5	63.5	58.9	52.4	49.9
	JUL20-2	141	94.5	83.5	97.5	83	97.5	112	93.4	92.8	93.9
Total R-factor (MJ mm ha^{-1} hr^{-1})	SEP19	57	628	90	1190	466	1109	517	607	956	970
	JUL20-1	114	51	136	33	61	34	34	64	42	41
	JUL20-2	385	211	148	316	187	594	350	216	274	371

Table 2. Correlations of the ^{137}Cs concentration in suspended solids (Cs_{ss}), dissolved ^{137}Cs concentration (Cs_{dis}), and apparent distribution coefficient (K_d) with representative physico-chemical properties

		^{137}Cs concentration in suspended solid (Cs_{ss}) (Bq kg^{-1})				Dissolved ^{137}Cs concentration (Cs_{dis}) (mBq L^{-1})						Apparent distribution coefficient K_d (L kg^{-1})					
		SSA (m^2 g^{-1})		TOC (%)		K^+ (mg L^{-1})		DOC (mg L^{-1})		EC (μS cm^{-1})		EC (μS cm^{-1})		TOC (%)		SSA (m^2 g^{-1})	
		n	*r*	*n*	*r*	*n*	*r*	*n*	*r*	*n*	*r*	*n*	*r*	*n*	*r*	*n*	*r*
Niida River	SEP19	6	0.28	6	0.51	6	-0.14	6	**0.85***	6	**-0.91***	6	-0.46	6	0.49	6	-0.27
	JUL20-1	6	-0.74	6	-0.46	6	0.41	6	0.37	6	-0.27	6	-0.40	5	-0.63	6	-0.79
	JUL20-2	7	-0.39	7	**0.77***	8	-0.15	8	0.17	8	**-0.75***	8	0.32	7	0.34	8	0.45
	Total	19	0.25	19	**0.60****	20	0.41	20	**0.69****	20	**-0.74****	20	-0.11	18	**0.47***	19	-0.04
Ukedo River	SEP19	6	0.25	5	**0.99****	6	-0.51	6	0.72	6	-0.27	6	-0.68	5	0.78	6	-0.39
	JUL20-1	6	0.54	6	**-0.87***	6	0.23	6	0.37	6	-0.08	6	-0.62	5	-0.78	6	-0.09
	JUL20-2	6	0.71	6	**-0.88***	7	0.54	7	0.17	7	-0.30	7	0.12	6	-0.29	6	-0.12
	Total	18	-0.01	17	**0.64***	19	**0.66****	19	**0.70****	19	0.19	19	-0.27	16	0.31	18	-0.14
Takase River	SEP19	6	-0.10	6	-0.05	6	-0.80	6	-0.81	6	**0.92****	6	-0.49	6	-0.49	6	0.22
	JUL20-1	6	-0.79	6	0.50	6	0.08	6	-0.39	6	0.72	6	-0.19	6	-0.54	6	0.04
	JUL20-2	7	-0.04	7	0.27	7	-0.52	7	**0.76***	7	**0.77***	7	-0.32	6	-0.51	7	-0.16
	Total	19	0.15	19	0.29	19	-0.21	19	-0.18	19	**0.62****	19	-0.46	18	0.08	19	0.36

* $p < 0.05$

** $p < 0.01$

Table 3. The suspended solid, particulate, dissolved, and total ^{137}Cs fluxes

River	Event	Suspended solid flux (Gg)	Particulate ^{137}Cs flux (GBq)	Dissolved ^{137}Cs flux (GBq)	Total ^{137}Cs flux (GBq)
Niida River	SEP19	2.12	18.8	0.137	19.0
	JUL20-1	0.135	1.50	0.074	1.57
	JUL20-2	1.69	6.04	0.086	6.13
Ukedo River	SEP19	0.113	5.39	0.273	5.67
	JUL20-1	0.017	0.227	0.098	0.325
	JUL20-2	0.019	0.269	0.096	0.365
Takase River	SEP19	2.17	13.1	0.096	13.2
	JUL20-1	0.193	0.655	0.061	0.717
	JUL20-2	0.558	2.24	0.079	2.32

Table 4. Results of desorption experiment and sequential extraction

	Sea water extraction (%)		Sequential extraction (%)		
Sample ID	30-min shaking	1-day shaking	Exchangeable fraction	Organic-bound fraction	Particle-bound fraction
ND-SEP19-4	2.8	3.3	2.5	2.5	95.1
UD-SEP19-3	5.1	6.6	5.0	5.5	89.6
TS-SEP19-4	2.6	3.4	2.9	3.0	94.2
ND-JUL20-2-5	2.1	2.8	2.6	3.2	94.3
TS-JUL20-2-4	2.8	3.2	4.1	5.9	90.0

Table 5. Estimated amount of ^{137}Cs desorbed from suspended solids in the ocean and the ratio of desorbed ^{137}Cs to dissolved ^{137}Cs.

Event	Desorbed ^{137}Cs in ocean (GBq)			Ratio of desorbed ^{137}Cs to dissolved ^{137}Cs		
	Niida River	Ukedo River	Takase River	Niida River	Ukedo River	Takase River
SEP19	0.57	0.33	0.42	5.2	1.5	6.2
JUL20-1	0.033	0.022	0.048	0.24	0.12	0.45
JUL20-2	0.25	0.030	0.19	0.90	0.15	1.2

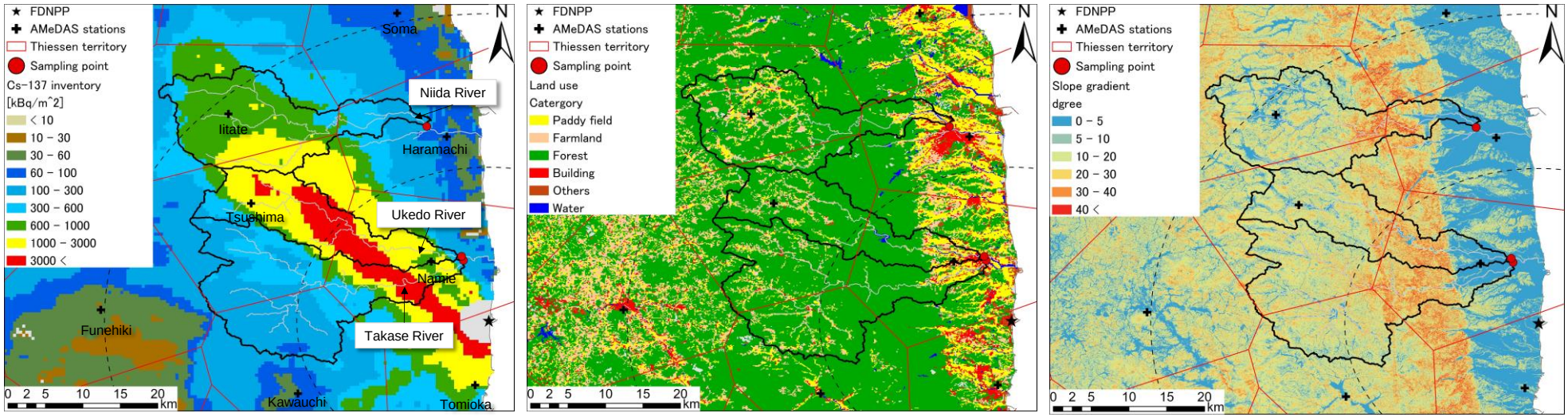

Figure 1. Spatial distribution of the ^{137}Cs inventory, land use, and slope gradient in the study catchments. The spatial distribution of the ^{137}Cs inventory is based on the fourth airborne survey by MEXT (2011). The Thiessen territory was created based on the coordination of Japan Meteorological Agency weather stations.

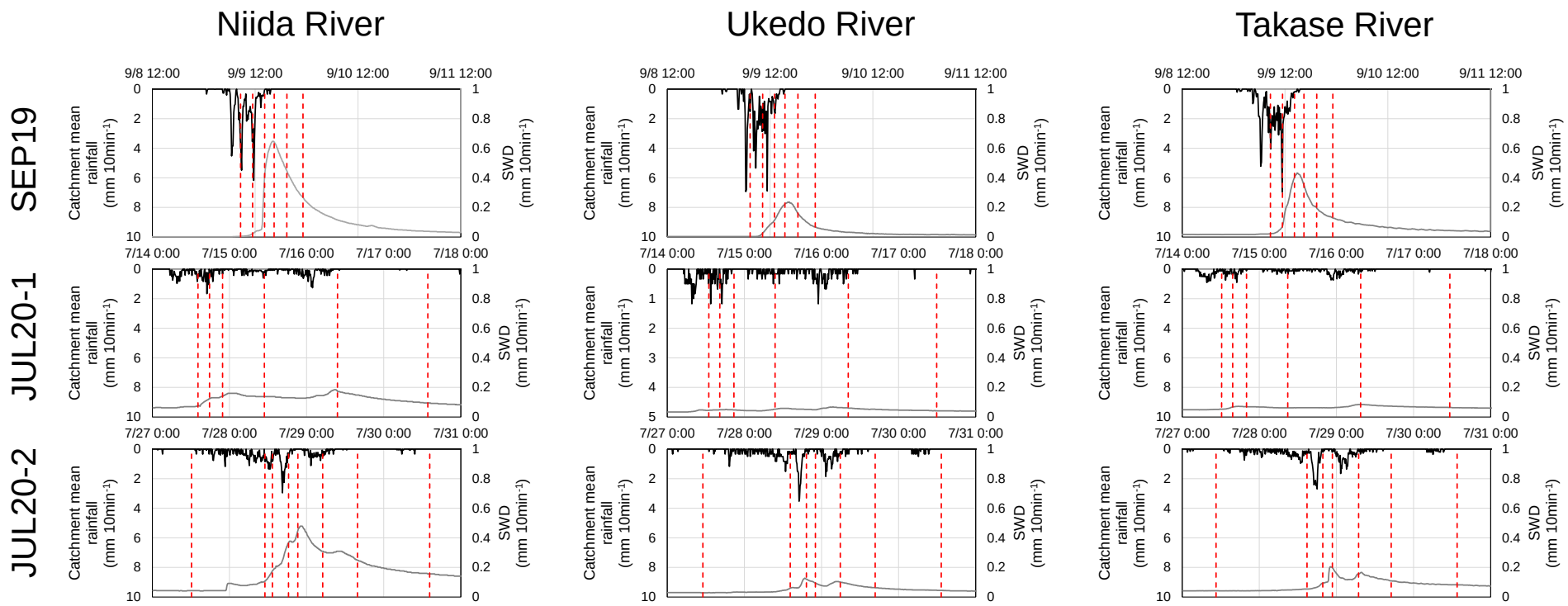

Figure 2. Sampling times (vertical dashed lines) of river water along with the hyetographs and hydrographs of the observed events. The hyetographs show the catchment mean rainfall amounts based on the Thiessen territory in Figure 1. The hydrograph shows the 10 minutes specific water discharge (SWD)

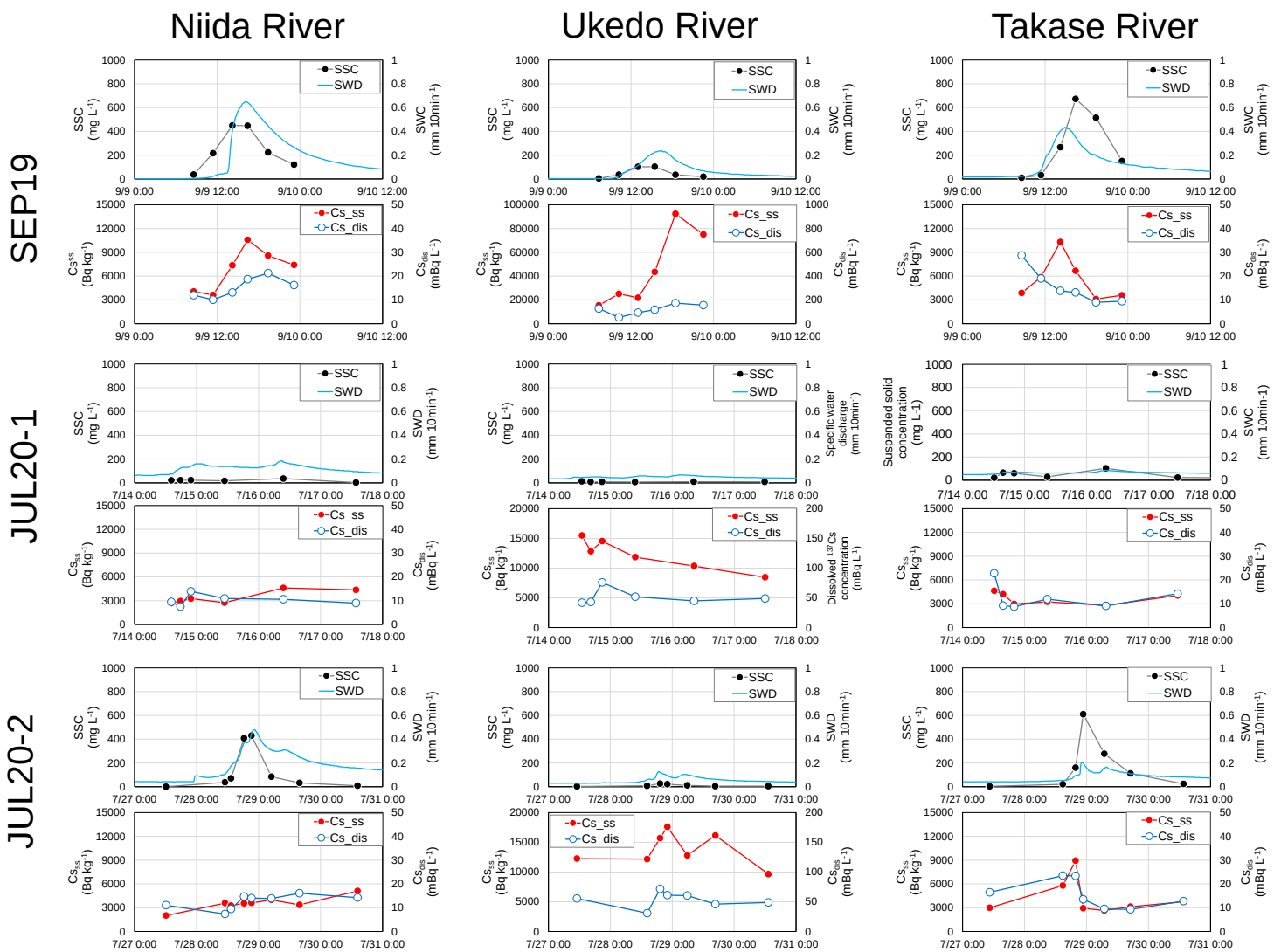

Figure 3. Temporal variations in the suspended solid concentration (SSC), ^{137}Cs concentration in suspended solids (Cs_{ss}), and dissolved ^{137}Cs concentration (Cs_{dis}) during the events.

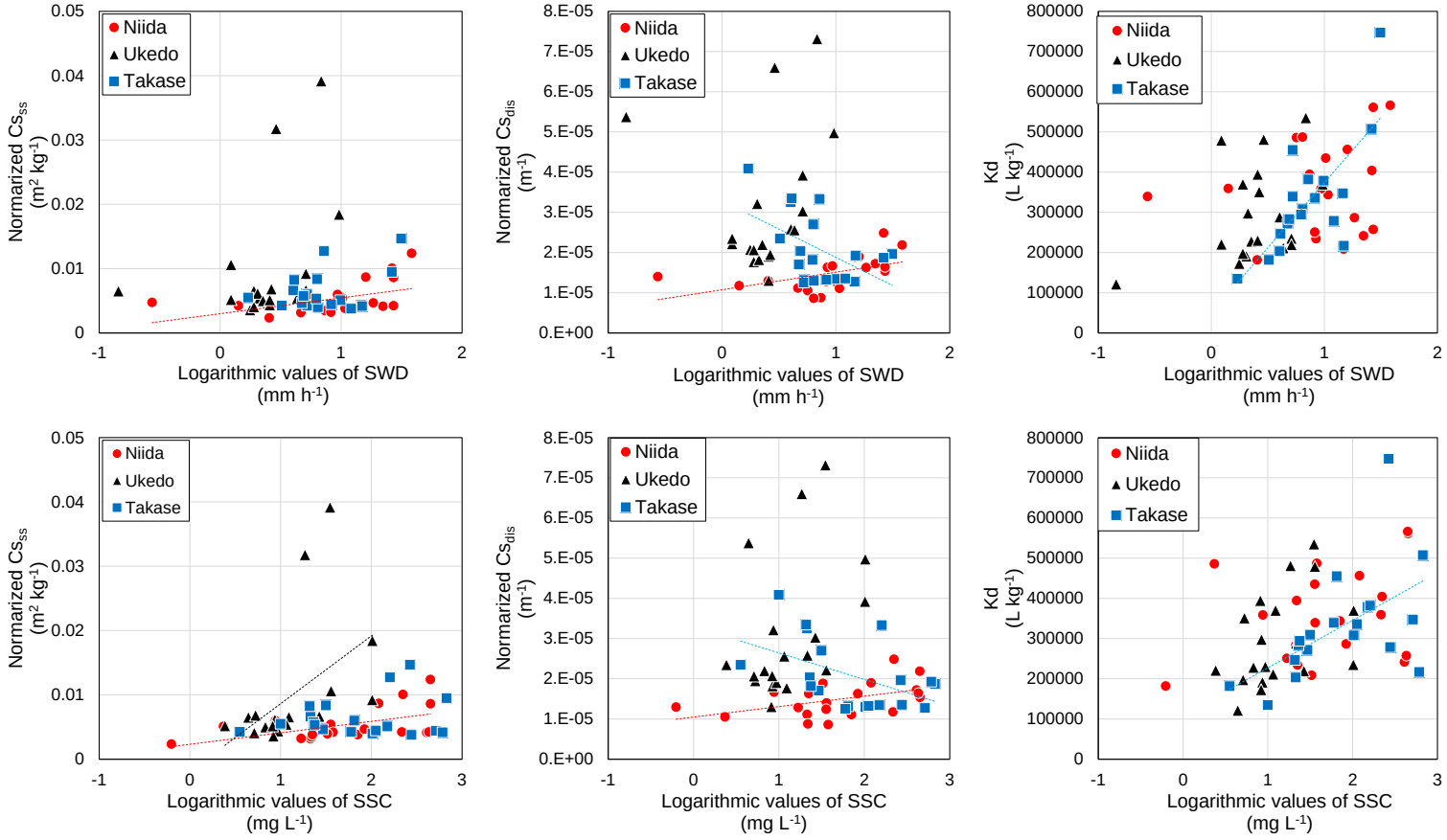

Figure 4. Scatterplots of the normalized ^{137}Cs concentration in suspended sediment (normalized Cs_{ss}), normalized dissolved ^{137}Cs concentration (normalized Cs_{dis}), and apparent distribution coefficient (K_d) versus the logarithms of the specific water discharge and suspended solid concentration. The normalized Cs_{ss} and normalized Cs_{dis} were obtained by dividing Cs_{ss} and Cs_{dis} by Catchment mean ^{137}Cs inventory, respectively. The specific water discharge every 10 minutes during sampling was multiplied by 6 to determine the hourly specific water discharge following Tsuji et al. (2016). Broken lines indicate significant correlations.

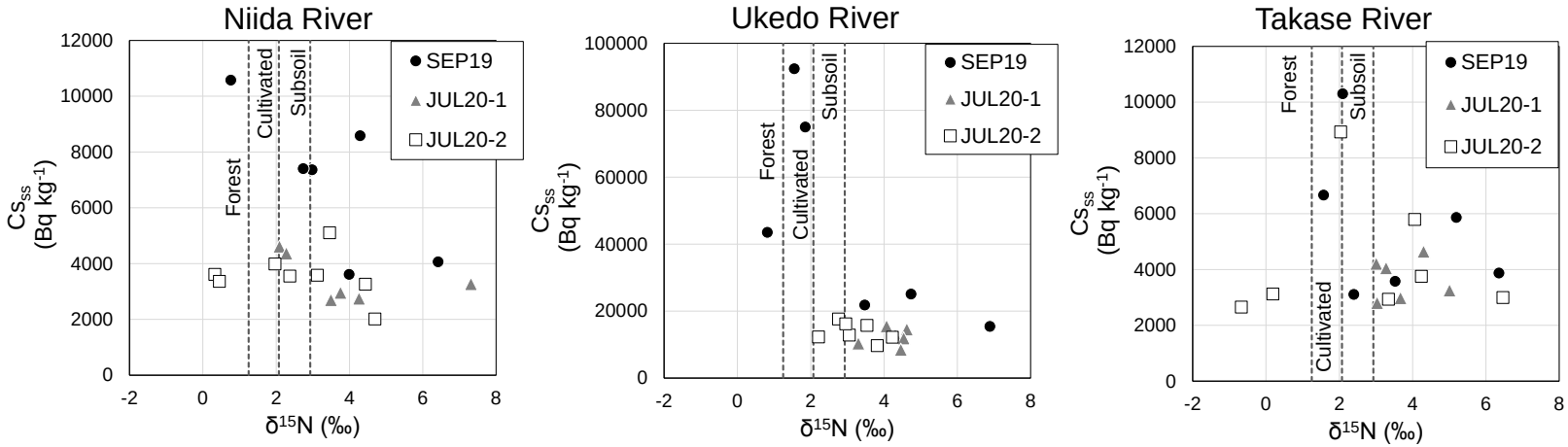

Figure 5. Relationship between the $\delta^{15}N$ and ^{137}Cs concentrations in suspended solids (Cs_{ss}). Broken lines represent the mean concentration of $\delta^{15}N$ in soil (< 2 mm), subsoil, cultivated land, and forest, according to Laceby et al. (2016a)

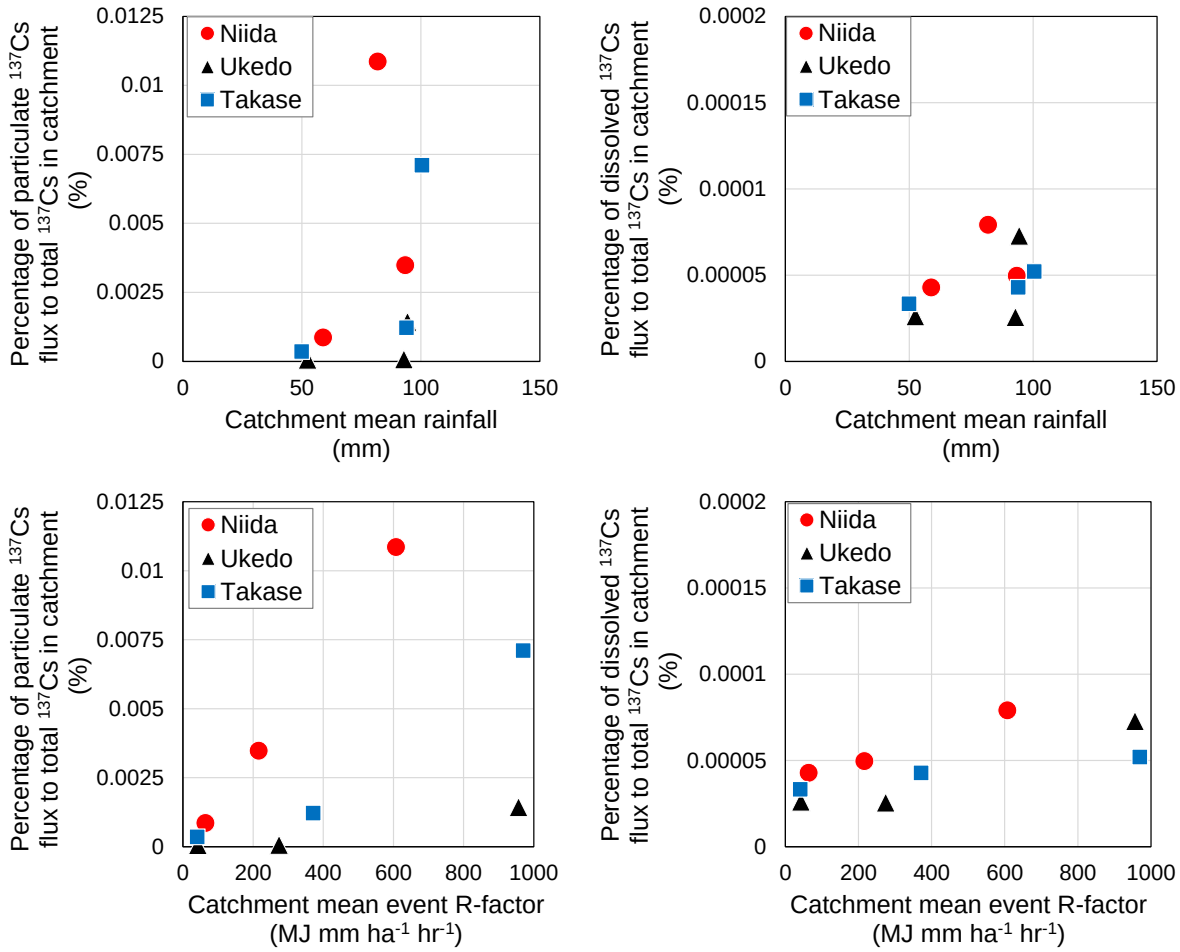

Figure 6. Scatterplots of the percentages of particulate and dissolved ^{137}Cs fluxes relative to the total ^{137}Cs in catchments, and the ratio of the particulate ^{137}Cs flux to the total ^{137}Cs flux versus the catchment mean rainfall and event R-factor.

Author Contributions Statement

Takuya Niida: Conceptualization, Methodology, Formal analysis, Investigation, Writing - Original Draft. **Yoshifumi Wakiyama:** Conceptualization, Formal analysis, Investigation, Writing - review & editing, Visualization. **Hyoe Takata:** Investigation, Writing - Review & Editing, Funding acquisition. **Keisuke Taniguchi:** Data curation, Writing - Review & Editing. **Honoka Kurosawa:** Investigation. **Kazuki Fujita:** Data curation, Resources. **Alexei Konoplev;** Writing - review & editing, Supervision, Funding acquisition